nature cell biology

Roles of ATM and NBS1 in chromatin structure modulation and DNA double-strand break repair

Elijahu Berkovich[1], Raymond J. Monnat, Jr.[2] and Michael B. Kastan[1,3]

We developed a novel system to create DNA double-strand breaks (DSBs) at defined endogenous sites in the human genome, and used this system to detect protein recruitment and loss at and around these breaks by chromatin immunoprecipitation (ChIP). The detection of human ATM protein at site-specific DSBs required functional NBS1 protein, ATM kinase activity and ATM autophosphorylation on Ser 1981. DSB formation led to the localized disruption of nucleosomes, a process that depended on both functional NBS1 and ATM. These two proteins were also required for efficient recruitment of the repair cofactor XRCC4 to DSBs, and for efficient DSB repair. These results demonstrate the functional importance of ATM kinase activity and phosphorylation in the response to DSBs, and support a model in which ordered chromatin structure changes that occur after DNA breakage depend on functional NBS1 and ATM, and facilitate DNA DSB repair.

DSBs can lead to mutations, chromosomal rearrangements and cell death. The main method used to study the binding of proteins to DSBs in mammalian cells uses fluorescent microscopy to analyse the formation of protein aggregates termed foci[1]. Analyses of damage-induced foci have provided useful information on the kinetics and colocalization of proteins in response to DNA damage. However, the interpretive power of this approach is limited by the low resolution of light microscopy, the large size of the foci and lack of evidence that foci selectively reflect protein binding to sites of DNA strand breaks. An alternative method that has facilitated the high-resolution analysis of protein recruitment to DSBs in yeast uses the HO mating-type switch endonuclease to introduce a DSB at a specific genomic site[2,3]. This system has been used in yeast to study the kinetics of recruitment of proteins to DSB sites, the response to DSBs and the molecular steps involved in DSB repair. The introduction of unique *ISce*I cleavage sites into the genomes of yeast[4] or human[5,6] cells has also been used to study DSB repair, but this approach requires the prior integration of the cleavage site into a host genome.

To analyze cellular responses to DSBs, including repair, at defined sites in human cells, we used the eukaryotic homing endonuclease I-PpoI, which has a 15 base pair recognition sequence[7,8], to cleave endogenous DNA target sites in the human genome. Expression of I-PpoI in human cells results in cleavage of ~10% of the 200–300 I-PpoI genomic target sites[9] to generate ~30 DSBs per cell (equivalent to that introduced by exposure to ~0.8 Gy irradiation). The dynamics and dependencies of DSB responses and DSB repair at these sites in human cells were examined.

Transient expression of I-PpoI in human cells resulted in measurable activation of the ATM signalling pathway and detectable specific binding of ATM and NBS1 to I-PpoI-induced DSBs in ChIP assays (see Supplementary Information, Fig. S1). The system was improved by adding a mutant oestrogen receptor hormone-binding domain to I-PpoI to create a fusion protein that could be localized to the nucleus in response to 4-hydroxytamoxifen (4-OHT)[10,11]. Addition of 4-OHT to MCF7 cells infected with an oestrogen receptor–I-PpoI retrovirus resulted in time-dependent cleavage of the endogenous 28S rDNA I-PpoI site (see Supplementary Information, Fig. S1e) and ATM activation (Fig. 1a). In these experiments, I-PpoI protein levels increased over time after addition of 4-OHT, most likely due to I-PpoI translocation to the nucleus with protection from proteasomal degradation (Fig. 1a). The 4-OHT-induced DSBs resulted in the expected ATM phosphorylation cascade (Fig. 1b and see Supplementary Information, Fig. S1a, c, d), and ATM, phosphorylated NBS1 and γH2AX could all be detected, by ChIP, adjacent to the DSB (Fig. 1c).

ATM exists as a homodimer (or higher-order oligomer) in unstressed human cells and irradiation causes dissociation of this dimer[12]. Dissociation requires both ATM kinase activity and intermolecular autophosphorylation of both ATM proteins on Ser 1981. After transfection of differentially epitope-tagged ATM proteins, we similarly found that dimeric ATM dissociates after I-PpoI-dependent DSB induction, and that the dissociation requires both ATM kinase activity and Ser 1981 phosphorylation (Fig. 1d). These results indicate that site-specific DSBs generated by I-PpoI recapitulate all key aspects of the induction of the ATM-dependent signalling pathway[13], thus permitting analysis of

[1]Department of Oncology, St. Jude Children's Research Hospital, Memphis, TN 38105, USA. [2]Departments of Pathology and of Genome Sciences, University of Washington, Box 357705, Seattle, WA 98195–7705, USA.
[3]Correspondence should be addressed to M.B.K. (e-mail: michael.kastan@stjude.org)

Received 5 March 2007; accepted 24 April 2007; published online 7 May 2007; DOI: 10.1038/ncb1599

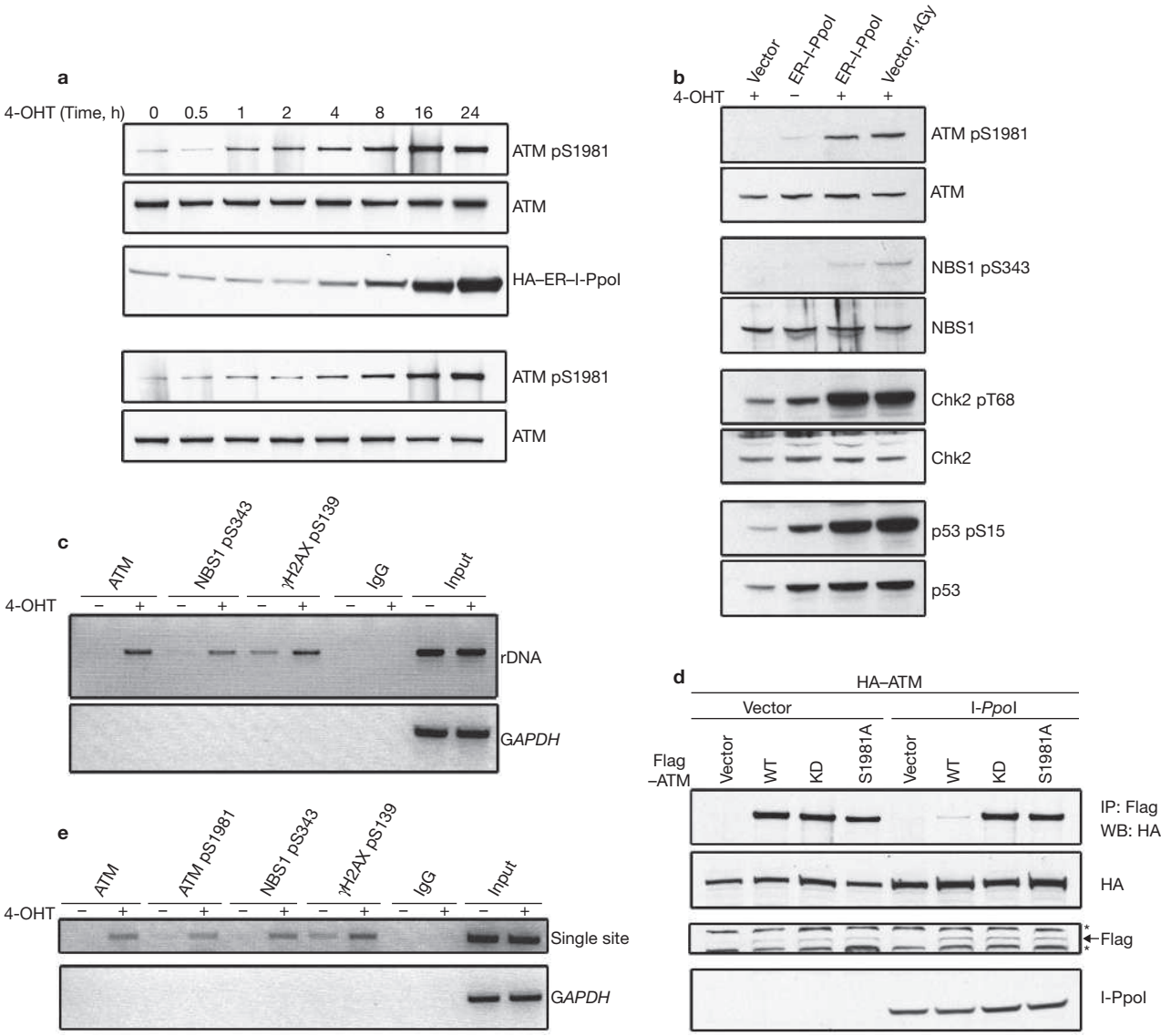

Figure 1 Characterization of I-PpoI-mediated DSB formation and damage response. (**a**) MCF7 cells were infected with a retrovirus harbouring HA–ER–I-PpoI. Twenty-four hours after infection, 4-OHT was added to cultures and cells were collected at the indicated times for western blot analysis. In parallel, MCF7 cells were irradiated at the indicated irradiation (IR) dose and collected 30 min after irradiation for western blot analysis. (**b**) MCF7 cells infected with HA–ER–I-PpoI were induced with 4-OHT for 8 h then collected and analysed by western blot for the indicated proteins. (**c**) Twenty-four hours after infection with HA–ER–I-PpoI, MCF7 cells were induced with 4-OHT for 16 h, fixed and subjected to a ChIP assay with oligonucleotides primers near the 28S rDNA target site (489 bp 3′ to I-PpoI cut site). *GAPDH* serves as a genomic DNA control as it has no I-PpoI site. (**d**) HA–ATM was coexpressed with either wild-type (WT) ATM, kinase-dead (KD) ATM (ATM^{KD}) or ATM^{S1981A} in ataxia-telangietasia (AT) fibroblasts (GM9607), with or without expression of I-PpoI. Twenty-four hours after transfection, ATM immunoprecipitated with anti-Flag was immunoblotted with an anti-HA antibody. Total cell extracts were also immunoblotted with anti-HA and anti-Flag antibodies to detect HA–ATM, Flag–ATM and HA–I-PpoI. Asterisks indicate non-specific bands. (**e**) Twenty four hours after infection with HA–ER–I-PpoI, MCF7 were induced with 4-OHT for 16 h, then fixed and subjected to ChIP analysis with oligonucleotide primer pairs adjacent to the single chromosome 1 I-PpoI cleavage site (280 bp 5′ to the I-PpoI cut site).

protein recruitment at a site-specific DSB. In contrast with focus formation, assessment of DSB binding in this assay is not dependent on antibody recognition of specific post-translational protein modifications.

In addition to the well-characterized target site for I-PpoI in the 28S ribosomal RNA gene, a unique cleavage site was identified in the human genome on chromosome 1 in an intron of the *DAB1* gene. The binding of damage-responsive proteins to DSBs at this chromosome 1 site was identical to 28S rDNA sites (Fig. 1e). This chromosome 1 site was used in most subsequent experiments to simplify analyses of protein recruitment to DSBs in human cells.

ATM autophosphorylation seems to be required for ATM activation after irradiation in human cells[12]. However, recent data have suggested that unphosphorylated ATM dimers can bind DNA to become activated *in vitro*[14], and the ATM pathway seems active in mice where the Atm autophosphorylation site is mutated[15]. The oestrogen receptor–I-PpoI system was used to directly explore the role of ATM kinase activity and ATM autophosphorylation in the DSB response in human cells. The specific ATM kinase inhibitor, KU55933 (ref. 16), inhibited I-PpoI-induced activation of ATM and its downstream substrates (Fig. 2a) and prevented detection of ATM protein at DSBs (Fig. 2b). NBS1 protein

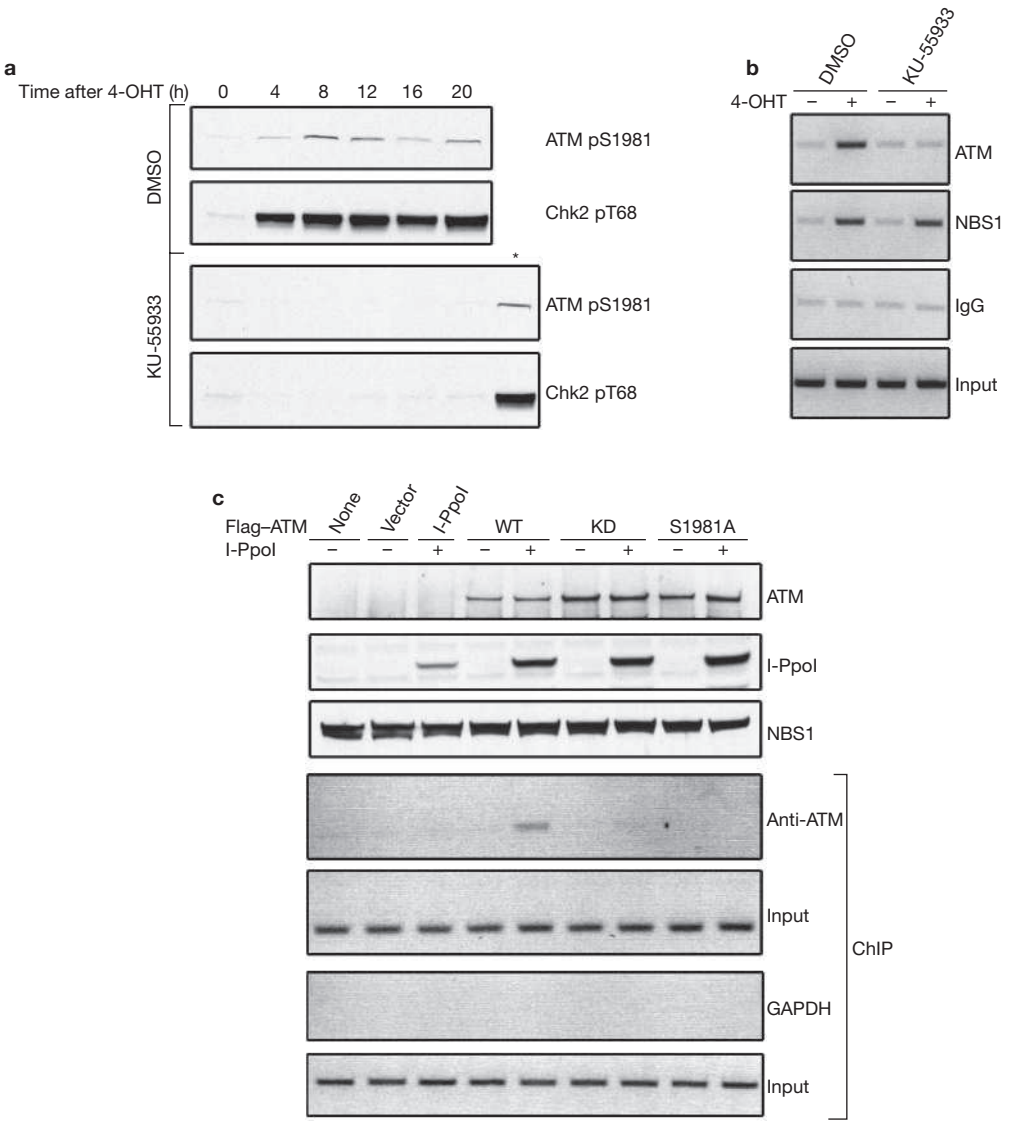

Figure 2 ATM dimers are not detected at DSB sites. (**a**) MCF7-cells infected with HA–ER–I-PpoI were induced with 4-OHT in the presence or absence of the ATM inhibitor KU-55933 (10 μM) for the indicated times. The cells were collected and proteins were analysed by western blot. The asterisk indicates positive control, same as 20 h DMSO. (**b**) MCF7 cells infected with HA–ER–I-PpoI were induced with 4-OHT in the presence or absence of KU-55933 (10 μM) for 12 h. Cells were then fixed and used for ChIP analysis with a primer pair 489 bp 3′ to the 28S rDNA I-PpoI cut site. (**c**) Wild-type ATM, ATM^{KD} or ATM^{S1981A} was expressed in AT fibroblasts (GM9607), with or without expression of I-PpoI. Twenty-four hours after transfection, cells were fixed and used for ChIP analysis with oligonucleotide primer pairs adjacent to the single chromosome 1 I-PpoI cleavage site (280 bp 5′ to the I-PpoI cut site; lower panel), or analysed by western blot (upper panel). *GAPDH* serves as a genomic DNA control where no I-PpoI site is available.

was detected at I-PpoI-induced DSBs independent of ATM activation or ATM recruitment. Similar results were obtained using the ATM inhibitor wortmannin at doses that inhibit cellular ATM, but not activity of the related kinase, ATR[17,12] (see Supplementary Information, Fig. S2). Thus, ATM kinase activity is required in human cells for both ATM dimer dissociation (Fig. 1d) and detectable binding of ATM protein to DSBs.

To further assess the roles of ATM activity and autophosphorylation in the binding of ATM at DSBs, the presence of transfected wild-type, kinase-inactive or ATM^{S1981A} proteins was examined at I-*Ppo*I-induced DSBs in ataxia-telangiectasia (AT) cells. Transgene-encoded ATM was the only source of ATM in these cells, thus permitting direct analysis of the requirement for ATM kinase activity and autophosphorylation to detect ATM at DSBs. Wild-type ATM, but neither kinase-inactive ATM nor ATM^{S1981A}, bound to I-PpoI-induced DSBs (Fig. 2c). Thus, ATM kinase activity and ATM activation with autophosphorylation are required to detect ATM at DSBs. Although it is not possible to exclude low level or transient binding of ATM^{S1981A} to DSBs that falls below the detection sensitivity of this assay, these differences in the DSB binding behaviour of wild-type versus mutant ATM^{S1981A} demonstrate that Ser 1981 phosphorylation is a determinant of ATM protein function in human cells.

DSBs can be repaired by nonhomologous end-joining (NHEJ), as well as by homologous recombination during the S and G2–M phases of the cell cycle. To assess the dynamics of protein recruitment and DSB repair during G1 when repair by NHEJ predominates,

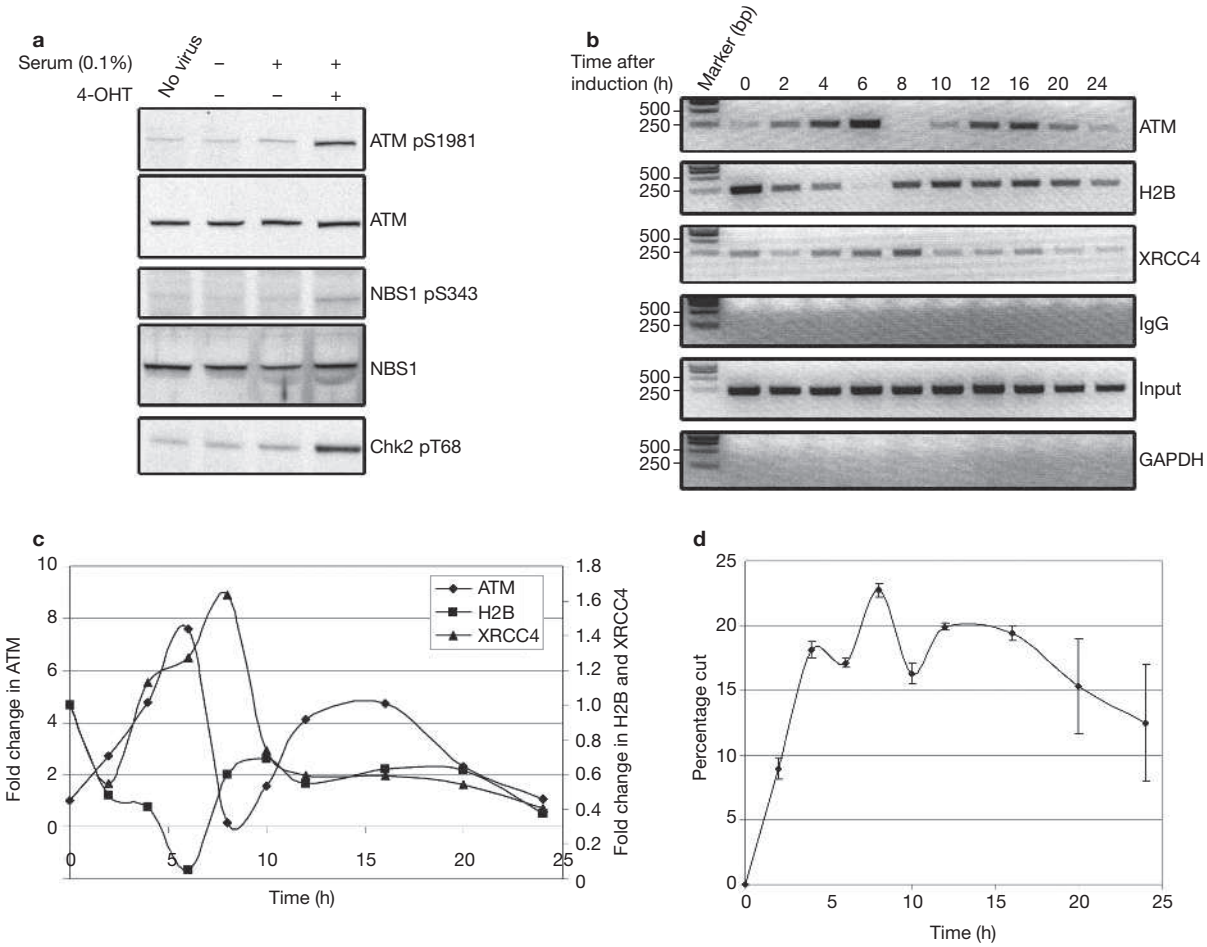

Figure 3 Detection, chromatin modulation and repair of a site-specific DSB. (**a**) MCF7 cells were infected with HA–ER–I-PpoI retrovirus, and 24 h after infection cells were transferred to media containing 0.1% FCS to accumulate cells in G1 (over 70% of cells in G1, as measured by flow cytometry) before I-PpoI induction for 12 h followed by western blot analysis for the indicated proteins. (**b**) As in **a**, but cells were induced with 4-OHT for the indicated times, then fixed and used for ChIP analyses using the indicated antibodies and a primer pair adjacent to the single chromosome 1 I-PpoI cleavage site (280 bp 5′ to the I-PpoI cut site) with the indicated antibodies. (**c**) Bands in **b** were quantified by densitometry using ImageJ for plotting. (**d**) Input DNA from **b** was used for real-time PCR with primers flanking the I-PpoI site at chromosome 1 (primer sets 6–17; see Supplementary Information, Table S1) or *GAPDH* as a control. ΔΔCT values were calculated and represented as a percentage of cut I-PpoI sites. Experiments were repeated three times, and the error bars represent mean ± s.d.

MCF7 cells were accumulated in G1 by serum starvation (>70%) before DSB induction. Serum starvation alone did not activate the ATM pathway, but DSB induction following 4-OHT addition activated ATM and its downstream targets (Fig. 3a). ChIP analyses of these synchronized cells revealed a time-dependent accumulation of ATM at DSBs and progressive histone 2B (H2B) loss from the DSB site, indicating nucleosomal disruption or loss. XRCC4, the requisite cofactor of DNA ligase 4 (Lig4) and NHEJ, was detected at the break site after ATM recruitment and H2B loss (Fig. 3b, c). To assess the corresponding time course of DSB generation and repair, I-PpoI-induced DSBs were monitored at the chromosome 1 site by quantitative real-time PCR analysis. DSBs were detected as early as 2 h after 4-OHT induction in conjunction with ATM recruitment and histone H2B loss, whereas DSB repair was detected at 8–10 hr in conjunction with XRCC4 recruitment to the DSB site (Fig. 3d). The persistence of DSBs up to 24 h after break induction seems to reflect persistence of active, nuclear-localized I-PpoI enzyme that retains the ability to recleave accurately repaired DSB sites.

Cells lacking full-length NBS1 protein had detectable, but low, levels of ATM activation after I-PpoI induction (see Supplementary Information, Fig. S3a), as we previously observed after irradiation-induced damage[18]. However, no ATM or activated ATM could be detected at DSBs by ChIP assay in the absence of full-length NBS1. The re-expression of wild-type NBS1 in these cells resulted in enhanced ATM activation and the recruitment of activated ATM to DSBs (see Supplementary Information, Fig. S3a, b). MRE11, which is part of the MRX complex in yeast, is important for histone loss from DSBs induced by HO endonuclease at the MATα locus[3]. Similarly, NBS1, a component of the analogous MRN complex in mammalian cells, was required for H2B loss at I-*Ppo*I-induced DSBs (Fig. 4a). Recruitment of XRCC4 was also significantly delayed in the absence of full-length NBS1. Complementation of NBS1-deficient cells with NBS1 restored I-PpoI-induced histone H2B loss, as well as recruitment of XRCC4 after induction of DSBs (Fig. 4a). Using a real-time PCR-based DSB repair-defect assay, higher levels of persistent DSBs were also detected in the absence of functional NBS1 compared to cells reconstituted with NBS1, indicating a repair defect in cells lacking full-length NBS1 (Fig. 4b).

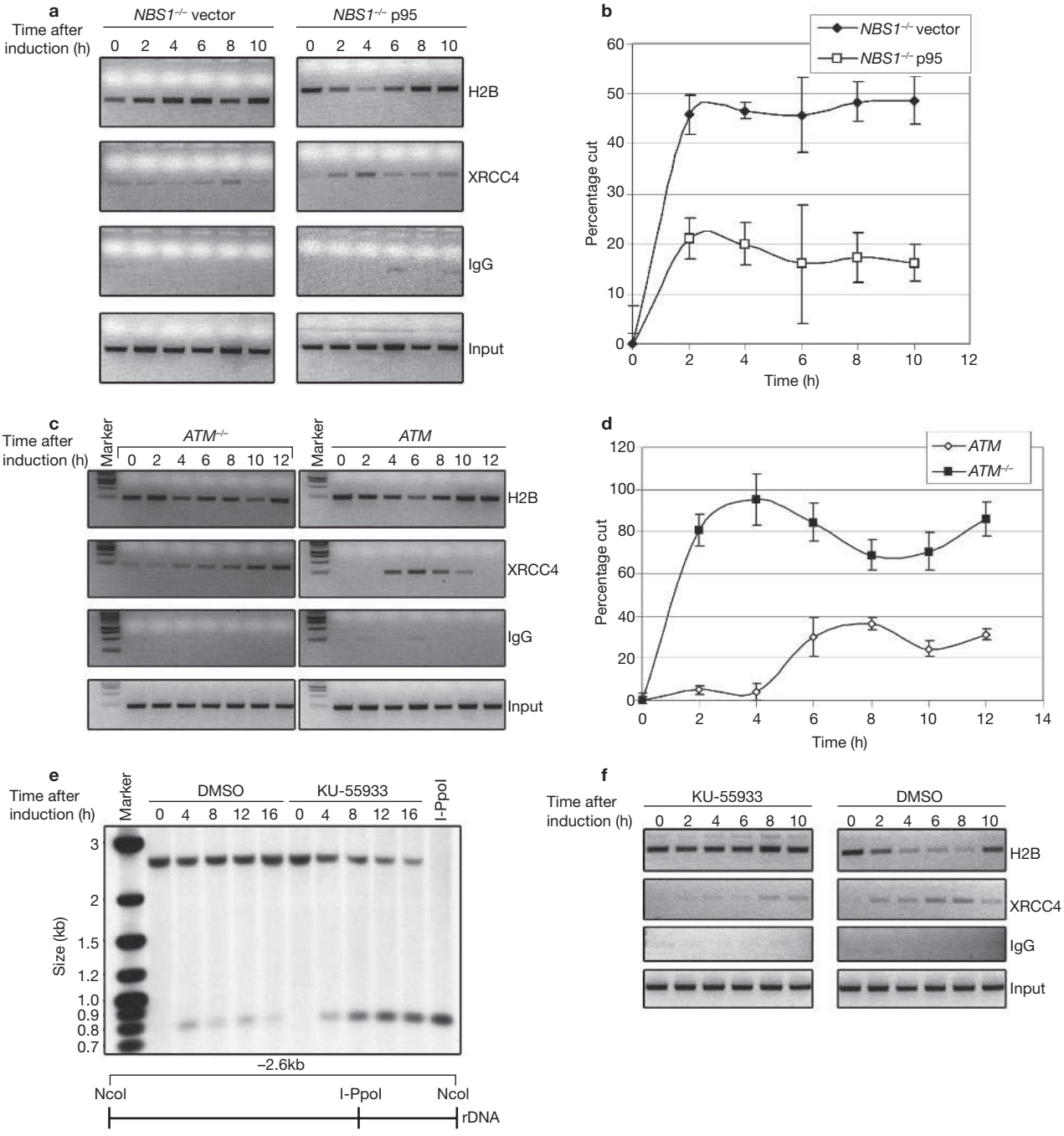

Figure 4 Histone loss from DSB sites and DSB repair are dependent on NBS1 and ATM. (**a**) *NBS1*-deficient ILB1 cells complemented with p95(NBS1) or a vector control were infected with HA–ER–I-PpoI retrovirus. Cells were induced with 4-OHT for the indicated times, then collected and used for ChIP analyses with the indicated antibodies and a primer pair adjacent to the single chromosome 1 I-PpoI cleavage site (280 bp 5′ to the I-PpoI cut site). (**b**) Input DNA from **a** was used for real-time PCR as in Fig. 3d. Experiments were repeated three times and error bars represent mean ± s.d. (**c**) *ATM*-null SV40-transformed fibroblasts (GM9607) and control SV40-transformed fibroblasts (GM0637) were infected with HA–ER–I-PpoI retrovirus. Cells were induced for indicated times, collected and used for ChIP analyses with the indicated antibodies using a primer pair adjacent to the single chromosome 1 I-PpoI cleavage site (280 bp 5′ to the I-PpoI cut site). (**d**) Input DNA from **c** was used for real-time PCR as in Fig. 3d. Experiments were repeated three times and the error bars represent mean ± s.d. (**e**) MCF7 cells infected with HA–ER–I-PpoI were induced in the presence or absence of KU-55933 (10 μM) for the indicated times. The cells were collected and genomic DNA was prepared using Puregene for Southern blot analysis of rDNA cleavage. I-PpoI cleavage generates a 0.8 kb cleavage fragment. I-PpoI-positive control of genomic DNA cut *in vitro* with *Nco*I followed by I-PpoI. (**f**) MCF7 cells treated as in **e** and used in a ChIP assay with the indicated antibodies and a primer pair adjacent to the single chromosome 1 I-PpoI cleavage site (280 bp 5′ to the I-PpoI cut site).

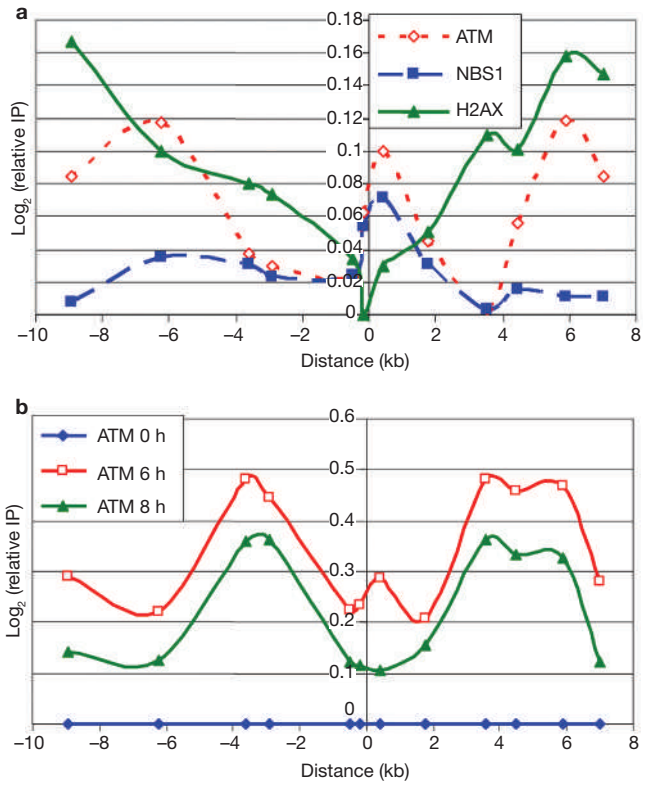

Figure 5 Distribution of damage response proteins around a site-specific DSB. (**a**) Relative ChIP values around the chromosome 1 DSB were determined using the indicated antibodies (ratio of sample to input calibrated to genomic *GAPDH*; see Methods and Supplementary Information, Table S1), as a function of distance from the DSB site 12 h after 4-OHT induction of I-PpoI. (**b**) DSB-specific relative ATM ChIP values as a function of time after induction of I-PpoI.

Unexpectedly, lack of ATM also resulted in reduced and asynchronous loss of H2B together with delayed recruitment of XRCC4 to DSB sites (Fig. 4c). *ATM*-null cells also had a defect in DSB repair, as reflected by higher DSB levels in *ATM*-null than in wild-type cells (Fig. 4d). To exclude the possibility that these differences in DSB repair in AT cells reflect the use of non-isogenic cell lines, the results were verified by using short interfering RNA (siRNA)-mediated *ATM* depletion from MCF7 cells (see Supplementary Information, Fig. S4). To further verify a DSB repair defect in cells lacking ATM function, a Southern blot assay was used to directly visualize the religation of I-PpoI-induced DSBs in 28S rRNA genes after inhibiting ATM kinase activity with KU-55933. Again, in the absence of ATM kinase activity the repair of I-PpoI-induced DSBs was significantly inhibited (Fig. 4e). Although only a fraction of the 28S rDNA I-PpoI sites are cleaved at any given time, the vast majority of rDNA sites seem to become cleaved over time in cells lacking ATM activity (Fig. 4e). ChIP analysis of cells lacking ATM activity reinforced the observation that nucleosome disruption and XRCC4 recruitment depend on ATM activity (Fig. 4f).

The large size of DNA damage-induced nuclear foci suggests that proteins are likely to be localized both at and adjacent to DSB sites. To gain insight into the recruitment and distribution of proteins at and around a site-specific DSB, we designed oligonucleotides for ChIP analysis on either side of the chromosome 1 I-PpoI break site. Although immunofluorescence staining for NBS1 and γH2AX after damage suggests their colocalization in nuclear foci[19], ChIP analysis revealed NBS1 was localized at the DSB site, whereas γH2AX accumulated adjacent to, but not directly at, the break site (Fig. 5a). Similar observations have been made about the distribution of γH2AX in yeast adjacent to HO-induced DSBs[20].

NBS1 and H2AX are both downstream targets of the ATM kinase, and ATM distribution around the DSB site coincided with the distribution of both phosphorylated H2AX and NBS1. ATM binding was detected in a surprisingly broad region flanking the DSB site, in addition to accumulating directly at the DSB site (Fig. 5a). As previously noted, ATM binding to the DSB site increased during the first 6 h after I-PpoI induction and then decreased at 8 h (Fig. 3b and c). In contrast, ATM protein remained bound on both sides of the DSB at 8 h. As XRCC4 is detected at the DSB site at 8 h (Fig. 3b) when ATM binding to the DSB had decreased (Fig. 5b), we speculate that ATM is either displaced by XRCC4 or leaves the break site by some other mechanism to allow access for DSB repair proteins.

We have developed a system to generate site-specific, chemically-defined DSBs at endogenous sites in the human genome, and have used this system to study the molecular events involved in the cellular response to DSB damage. This system allowed us to confirm several features of the response to DSBs, and to identify several novel features of the DSB response in human cells. This system has advantages over the previously reported use of ISceI sites[4,5,6]: first, I-PpoI sites are defined, endogenous DSB sites, precluding the need to introduce DSB sites into cells before experiments; second, evolutionary conservation of the endogenous I-PpoI sites permits DSBs to be introduced and assays to be performed in virtually any eukaryotic species, cell type or genetic background; and third, as I-PpoI induces multiple DSBs in contrast with the 1–2 DSBs typically introduced in ISceI-transfected cells, the entire ATM signalling pathway is activated and thus can be studied.

Our results identified clear parallels with previous work on HO endonuclease-induced DSBs at the MAT locus in yeast[2,3]. For example, we identified a role for the MRN complex in histone loss at break sites similar to what had been observed for the yeast MRX complex. One conspicuous difference between our analyses of DSB repair in human cells and corresponding analyses of HO-induced DSB repair in yeast at the MAT locus, is the occurrence of continuous resection of the broken DNA after HO cleavage. This extensive resection is likely to provide yeast with a different molecular substrate for DSB responses and repair, in contrast with the limited resection that seems to follow I-PpoI-induced DSBs. In addition, the functional roles of ATM and NBS1 cannot be directly analysed in yeast, which lack both proteins.

Using I-PpoI-induced DSBs, we were able to confirm that NBS1 protein was required to recruit ATM to DSBs, as had been previously suggested by less definitive assays[18,21]. We were also able to extend previous immunofluorescence-based focus-forming assays[22] by showing that inactive or unphosphorylated ATM does not detectably bind to DSBs in human cells. These results differ from interpretations of recent *in vitro* data suggesting that nonphosphorylated ATM may bind to and be activated by DNA ends[14], and experiments using laser microbeam-induced damage that suggested that nonphosphorylatable mouse Atm can accumulate at sites of DNA damage[15]. Overexpression of ATM in our system would not account for these differences, as overexpression artifacts should lead to the opposite of what we observed, by promoting the inappropriate binding or activation of ATM. Clear differences between the behaviour of wild-type human ATM protein in our assays compared with either

kinase-inactive or mutant ATM^{S1981A} proteins demonstrate the functional importance of both the ATM kinase activity and autophosphorylation in the ATM-mediated response to DSBs in human cells.

ATM protein can be activated, albeit at low levels, in the absence of detectable DSBs[12,18,23,24]. These observations are consistent with a model in which chromatin structure changes can initiate ATM activation. The low level of ATM activation following such treatments (for example, hypotonic swelling or chloroquine treatment) is similar to that observed after introduction of DSBs in cells lacking NBS1 protein[18]. In both settings, ATM is activated at a low level and nucleoplasmic substrates like p53 are phosphorylated. However, there is no phosphorylation of proteins at DSB sites (for example, NBS1 or SMC1). Our new findings illustrate one type of NBS1-dependent chromatin structure change – nucleosomal alteration leading to histone loss – that may quantitatively contribute to complete activation of the ATM protein.

Although nucleosome disruption has been well-documented during nucleotide-excision repair[25], nucleosome disruption during DSB repair in human cells has not been clearly demonstrated. Our results document nucleosomal changes during DSB repair, and indicate that NBS1 and ATM proteins are critically important for these changes to occur. Cells lacking functional NBS1 or ATM fail to display efficient histone loss from DSB sites, and exhibit a concomitant failure to efficiently recruit proteins for DSB repair. These data suggest a dynamic series of molecular events that modulate chromatin structure to influence DNA DSB repair (see Supplementary Information, Fig. S4), and provide an explanation for how NBS1 or ATM deficiency leads to defects in DSB repair and damage-dependent signalling in human cells. As the target site for the I-PpoI homing endonuclease is a highly conserved 15 base pair sequence found in virtually all eukaryotic genomes, it should be possible to extend the system described here to further elucidate mechanistic details of the response to DSB damage in many organisms. □

METHODS

Expression constructs. I-PpoI expression plasmids were previously described[9]. The open reading frame of I-PpoI was amplified by PCR and the BglII fragment was ligated into pBABE–HA–ER–E7 (ref. 11) cut with BamHI to maintain the reading frame with HA–ER. The construct was verified by sequencing, and protein expression was verified by western blot. Expression vectors for wild-type ATM, kinase-inactive ATM and ATM^{S1981} were previously reported[12]. An HA–ATM expression plasmid was a gift from R. Tibbetts.

Cell culture, transfections, siRNA and retroviral infection. MCF7, HeLa, HEK293T, AT fibroblasts GM9607 and GM0637 and NBS-ILB1 cells[26] were grown in DMEM supplemented with 10% FBS at 37 °C in a humidified atmosphere containing 5% CO_2. Serum starvation was done in media containing 0.1% FBS for 24 hr. 4-OHT (Sigma, St Louis, MO) was added to a final concentration of 1 μM for up to 24 h to induce the nuclear localization of ER–I-PpoI protein. Wortmannin (30 μM, Sigma) was added every 2 h for a total of 8 h because of its short half-life in culture medium (see Supplementary Information, Fig. 2a). The ATM inhibitor KU-55933 (K4014, Sigma) was prepared as 10 mM stock solution in DMSO and used at 10 μM final concentration. Ionizing irradiation from a ^{137}Cs source was delivered at a rate of 120 cGy min^{-1}. Transient plasmid transfections were performed using Effectene (Qiagen, Hilden, Germany), whereas *ATM* siRNA (Dharmacon, SmartPool ATM - L-003201-00-0020) and control siRNA transfections were performed using siPORT *NeoFX* (Ambion, Austin, TX) following the manufacturer's protocol. Sequences were as follows: Dharmacon ATM siRNA (pool of four oligonucleotides: GCAAAGCCCUAGUAAAUAUU; GGUGGAUCUUCAGUAUAUUU; GAGAGGAGACAGCUUGUUAUU; GAUGGGAGGCCUAGGAUUUUU) and Ambion non-targeting control #1, AGUACUGCUUACGAUACGGdTdT. HA–ER–IPpo1 retrovirus was prepared and used in infection essentially as previously described[27].

Western blots, southern blot, immunofluorescence microscopy and antibodies. Cells were harvested and lysed in TGN buffer (50 mM Tris–HCl at pH 7.5, 150 mM NaCl, 1% Tween 20, 0.5% NP40, 1× proteinase inhibitor cocktail; Roche, Mannheim, Germany) for immunoprecipitation, or in RIPA buffer (200 mM NaCl, 10 mM Tris–HCl at pH 7.5, 0.1% SDS, 1% Triton X-100, 1% deoxycholate, 5 mM EDTA, 1× proteinase inhibitor cocktail) for western blot analyses. The protein concentration of cleared lysates was determined (DC; BioRad, Hercule, CA) before electrophoresis through PAGE gels (NuPAGE; Invitrogen, Carlsbad, CA) followed by transfer onto nitrocellulose membranes for antibody probing. Antibodies used were: anti-ATM (MAT3; gift from Y. Shiloh, Tel-Aviv, Israel), anti-ATMphosphoSer 1981 (ref. 12), anti-NBS1 (NB 100-143; Novus, Littleton, CO), anti-NBS1S343p (3001; Cell Signaling, Danvers, MA), anti-Chk2 (sc-17747; Santa-Cruz, Santa Cruz, CA), anti-Chk2T68p (2661, Cell Signaling), anti-p53 (sc-6243, Santa-Cruz), anti-p53S15p (9248, Cell Signaling), anti-HA (MMS-101R; Covance, Berkeley, CA), anti-Flag M5 (F-4042, Sigma), anti-α-tubulin (T9026, Sigma,) and anti-γH2AXS139p (07-164; Upstate, Walthers, MA). Immunofluorescence microscopy assays were performed as previously described[18]. For Southern blots, cells expressing ER–I-PpoI were induced for the indicated times and genomic DNA was prepared using Puregene (D-5000A; Gentra, Minneapolis, MN) according to the manufacturer's instructions. DNA was cut with NcoI (15421-050, Invitrogen) resulting in a ~2.6 kb rDNA fragment in which the I-PpoI site is located 0.8 kb 5′ to the 3′ end of the rDNA fragment (see Fig. 4e). For each time point, 5 μg of genomic DNA was fractionated by electrophoresis through a 1% agarose gel and transferred to a Biodyne B membrane (60-00-50; KPL, Gaithersburg, MD). Membrane bound rDNA fragments were detected by Detector AP chemiluminescent blotting kit (54-30-02, KPL,) according to manufacturer's instructions. The rDNA hybridization probe consisted of 199 bp 3′ to the rDNA I-PpoI cleavage site. The rDNA probe was biotin labelled using PCR DNA biotinylation kit (60-0101, KPL,) using oligonucleotides 1B (see Supplementary Information, Table S1).

Chromatin immunoprecipitation. For each precipitation, 1×10^7 cells were crosslinked by the addition of formaldehyde directly to the growth medium to a final concentration of 0.5%. Crosslinking was stopped after 10 min at room temperature by the addition of glycine to a final concentration of 0.125 M. Crosslinked cells were washed with PBS, scraped, washed with PBS with 1 mM PMSF, then resuspended in 2 ml buffer I (10 mM HEPES at pH 6.5, 10 mM EDTA, 0.5 mM EGTA, 0.25% Triton X-100 supplemented with phosphatase/protease inhibitors: 1 mM PMSF; 1 μg ml^{-1} leupeptin, L-2884, Sigma; and 20 μg ml^{-1}aprotinin, A6279, Sigma). Cells were pelleted by centrifugation and then resuspended in 2 ml buffer II (10 mM HEPES at pH 6.5, 1 mM EDTA, 0.5 mM EGTA, 200 mM NaCl and phosphatase/protease inhibitors). After centrifugation, nuclei were resuspended in 0.3–1 ml lysis buffer (50 mM Tris at pH 8.1, 10 mM EDTA, 1% SDS and phosphatase/protease inhibitors). The resulting chromatin was sonicated to an average size of 1000 bp, then microcentrifuged. The supernatant was diluted (between 1:5 to 1:10 with 10 mM Tris, at pH 8.1, 150 mM NaCl, 2 mM EDTA and 1% Triton X-100), and 1% of the diluted supernatant was taken for protein and DNA concentration measurements. The same amount of protein–DNA from each sample was used for immunoprecipitations. After preclearing with BSA–IgG–t-RNA-blocked protein-A/G agarose beads, 2–3 μg antibody was added to each aliquot of chromatin and incubated on a rotating platform overnight at 4 °C. Immunocomplexes were recovered with BSA–t-RNA-blocked protein-A/G agarose beads. Following extensive washing, bound DNA fragments were eluted, purified and analysed by PCR or by SyberGreen (Applied Biosystems, Foster City, CA) real-time PCR. SyberGreen real-time PCR dissociation curves showed that each primer set gave a single and specific product. The antibodies used were anti-ATM (AB3, PC116-Calbiochem), anti-NBS1 (NB 100-143, Novus), anti-NBS1S343p (3001, Cell Signaling), anti-γH2AXS139p (07-164, Upstate,), anti-ATM1981S-P[12], anti-XRCC4 (ab145; Abcam, Cambridge, MA) and anti-H2B (07-371, Upstate,). Sequences of primers used for PCR and real-time PCR are given in the Supplementary Information, Table S1. Experiments were repeated at least twice and, in each real-time PCR experiment, reactions were performed in duplicate.

I-PpoI sites in the human genome. The 28S human rDNA I-PpoI site is located in rDNA sequence accession# U13369 (Genbank) at nucleotides 11680–11695. The human chromosome 1 I-PpoI site is located at 1p32.2 in an intron of the *DAB1*

gene (GeneID 1600 Enterz Gene). To amplify this region containing the I-PpoI site, primers corresponding to Ensembl database contig# AL391826.7.1.68224 nucleotides 35343 to35357 on the plus strand were used.

Data analysis. Relative immunoprecipitation values represent the ratio of immunoprecipitated DNA as determined by real-time PCR to *GAPDH* input DNA before induction, normalized to the ratio immunoprecipitated DNA to *GAPDH* input DNA after induction of I-PpoI. Primers are detailed in the Supplementary Information, Table S1 — oligonucleotides for real-time PCR protein distribution assay (I-PpoI cut site at 10000bp). Primers (see Supplementary Information, Table S1; oligonucleotides for real-time PCR repair assay) flanking the I-Ppo1 site at chromosome 1 and *GAPDH* as an internal control were used to determine the extent of I-PpoI DSB generation and repair. Input DNA from ChIP assays was used for SyberGreen real-time PCR. Percentage of cut was calculated using the ΔΔCT method (Applied Biosystems; http://docs.appliedbiosystems.com/pebiodocs/04371095.pdf). s.d. was calculated from triplicate samples in the real-time PCR.

Note: Supplementary Information is available on the Nature Cell Biology website.

ACKNOWLEDGMENTS

We thank D. Woods and M. Reis for excellent technical assistance. This work was supported by grants from the National Institutes of Health (CA71387 and CA21765 to M.B.K. and CA48022 to R.J.M., Jr.) and by the American Lebanese Syrian Associated Charities (ALSAC) of the St. Jude Children's Research Hospital.

COMPETING FINANCIAL INTERESTS

The authors declare that they have no competing financial interests.

Published online at http://www.nature.com/naturecellbiology/
Reprints and permissions information is available online at http://npg.nature.com/reprintsandpermissions/

1. Paull, T. T. *et al.* A critical role for histone H2AX in recruitment of repair factors to nuclear foci after DNA damage. *Curr. Biol.* **10,** 886–895 (2000).
2. Rudin, N. & Haber, J. E. Efficient repair of HO-induced chromosomal breaks in *Saccharomyces cerevisiae* by recombination between flanking homologous sequences. *Mol. Cell Biol.* **8,** 3918–3928 (1988).
3. Tsukuda, T., Fleming, A. B., Nickoloff, J. A. & Osley, M. A. Chromatin remodelling at a DNA double-strand break site in *Saccharomyces cerevisiae*. *Nature* **438,** 379–383 (2005).
4. Lisby, M., Barlow, J. H., Burgess, R. C. & Rothstein, R. Choreography of the DNA damage response: spatiotemporal relationships among checkpoint and repair proteins. *Cell* **118,** 699–713 (2004).
5. Richardson, C. & Jasin, M. Frequent chromosomal translocations induced by DNA double-strand breaks. *Nature* **405,** 697–700 (2000).
6. Rodrigue, A. *et al.* Interplay between human DNA repair proteins at a unique double-strand break *in vivo*. *EMBO J.* **25,** 222–231 (2006).
7. Muscarella, D. E., Ellison, E. L., Ruoff, B. M. & Vogt, V. M. Characterization of I-Ppo, an intron-encoded endonuclease that mediates homing of a group I intron in the ribosomal DNA of *Physarum polycephalum*. *Mol. Cell Biol.* **10,** 3386–3396 (1990).
8. Flick, K. E., Jurica, M. S., Monnat, R. J., Jr. & Stoddard, B. L. DNA binding and cleavage by the nuclear intron-encoded homing endonuclease I-PpoI. *Nature* **394,** 96–101 (1998).
9. Monnat, R. J., Jr., Hackmann, A. F. & Cantrell, M. A. Generation of highly site-specific DNA double-strand breaks in human cells by the homing endonucleases I-PpoI and I-CreI. *Biochem. Biophys. Res. Commun.* **255,** 88–93 (1999).
10. Vigo, E. *et al.* CDC25A phosphatase is a target of E2F and is required for efficient E2F-induced S phase. *Mol. Cell Biol.* **19,** 6379–6395 (1999).
11. Berkovich, E., Lamed, Y. & Ginsberg, D. E2F and Ras synergize in transcriptionally activating p14ARF expression. *Cell Cycle* **2,** 127–133 (2003).
12. Bakkenist, C. J. & Kastan, M. B. DNA damage activates ATM through intermolecular autophosphorylation and dimer dissociation. *Nature* **421,** 499–506 (2003).
13. Kastan, M. B. & Bartek, J. Cell-cycle checkpoints and cancer. *Nature* **432,** 316–323 (2004).
14. Lee, J. H. & Paull, T. T. ATM activation by DNA double-strand breaks through the Mre11–Rad50–Nbs1 complex. *Science* **308,** 551–554 (2005).
15. Pellegrini, M. *et al.* Autophosphorylation at serine 1987 is dispensable for murine Atm activation *in vivo*. *Nature* **443,** 222–225 (2006).
16. Hickson, I. *et al.* Identification and characterization of a novel and specific inhibitor of the ataxia-telangiectasia mutated kinase ATM. *Cancer Res.* **64,** 9152–9159 (2004).
17. Sarkaria, J. N. *et al.* Inhibition of phosphoinositide 3-kinase related kinases by the radiosensitizing agent wortmannin. *Cancer Research* **58,** 4375–4382 (1998).
18. Kitagawa, R., Bakkenist, C. J., McKinnon, P. J. & Kastan, M. B. Phosphorylation of SMC1 is a critical downstream event in the ATM–NBS1–BRCA1 pathway. *Genes Dev.* **18,** 1423–1438 (2004).
19. Bekker-Jensen, S. *et al.* Spatial organization of the mammalian genome surveillance machinery in response to DNA strand breaks. *J. Cell Biol.* **173,** 195–206 (2006).
20. Shroff, R. *et al.* Distribution and dynamics of chromatin modification induced by a defined DNA double-strand break. *Curr. Biol.* **14,** 1703–1711 (2004).
21. Falck, J., Coates, J. & Jackson, S. P. Conserved modes of recruitment of ATM, ATR and DNA-PKcs to sites of DNA damage. *Nature* **434,** 605–611 (2005).
22. Young, D. B. *et al.* Identification of domains of Ataxia-telangiectasia Mutated required for nuclear localization and chromatin association. *J. Biol. Chem.* **280,** 27587–27594 (2005).
23. Collis, S. J. *et al.* Evasion of early cellular response mechanisms following low level radiation-induced DNA damage. *J. Biol. Chem.* **279,** 49624–49632 (2004).
24. Difilippantonio, S. *et al.* Role of Nbs1 in the activation of the Atm kinase revealed in humanized mouse models. *Nature Cell Biol.* **7,** 675–685 (2005).
25. Gong, F., Kwon, Y. & Smerdon, M. J. Nucleotide excision repair in chromatin and the right of entry. *DNA Repair* **4,** 884–896 (2005).
26. Lim, D.-S. *et al.* ATM phosphorylates p95/nbs1 in an S-phase checkpoint pathway. *Nature* **404,** 613–617 (2000).
27. Berkovich, E. & Ginsberg, D. Ras induces elevation of *E2F-1* mRNA levels. *J. Biol. Chem.* **276,** 42851–42856 (2001).

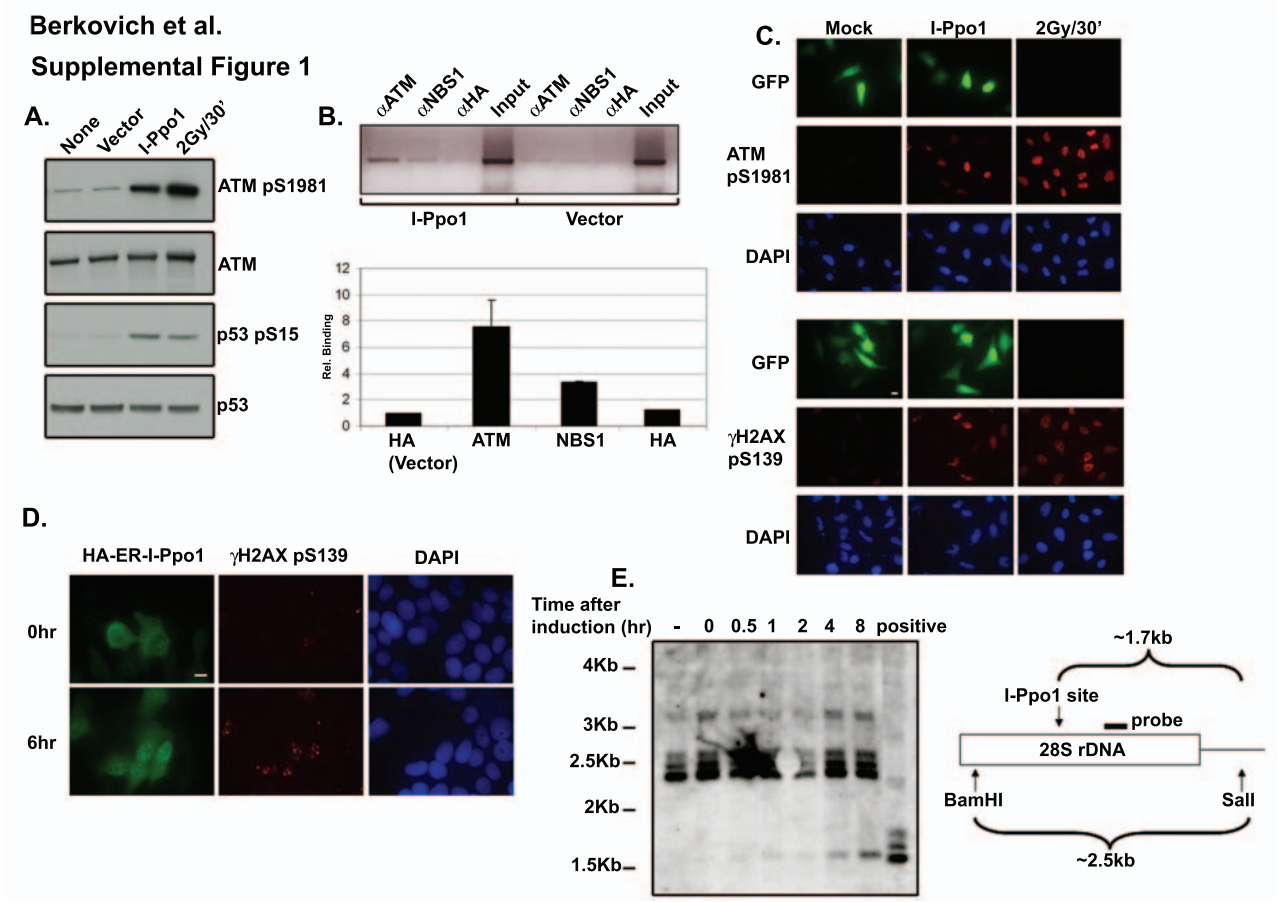

Figure S1: Activation of the ATM pathway by I-PpoI. **A.** HEK293T cells were either untransfected, vector transfected, transfected with an I-PpoI expression vector, or subjected to 2Gy γ-irradiation. 24 hrs after transfection or treatment, cellular proteins were analyzed by Western blot using the indicated antisera. **B.** HEK293T cells were transfected with vector or with an I-PpoI expression vector, and 24 hrs after transfection cells were fixed with formaldehyde and collected for ChIP analysis at the rDNA site (489bp 3' to I-PpoI cut site). (upper panel). ChIP samples were used in real time PCR quantification of relative binding to the site of damage (lower panel). The HA-tag-immunoprecipitated ChIP sample from vector transfected cells was assigned a value of 1. Experiment was repeated twice, data are mean ± standard deviation **C.** HeLa cells transfected with either a GFP expression vector or with GFP and I-PpoI expression vectors were harvested 24 hrs after transfection and prepared for immunofluorescence microscopy. As a positive control, cells were irradiated with 2Gy, then fixed after 30 min. **D.** HA-ER-I-PpoI-infected MCF7 cells were induced with 4-OHT for 6hrs, then fixed and stained with antisera against the indicated proteins prior to immunofluorescence microscopy. Approximately 15-20 γH2AX foci are seen in each nucleus, some foci representing multiple DSBs clustered in rDNA. **E.** MCF7 cells were infected with HA-ER-I-PpoI and induced with 4-OHT for the indicated times prior to genomic DNA isolation. DNAs were digested with *BamH*I/*Sal*I prior to Southern blot analysis using a 28S rDNA probe. Positive – genomic DNA digested with *BamH*I/*Sal*I followed by I-PpoI.

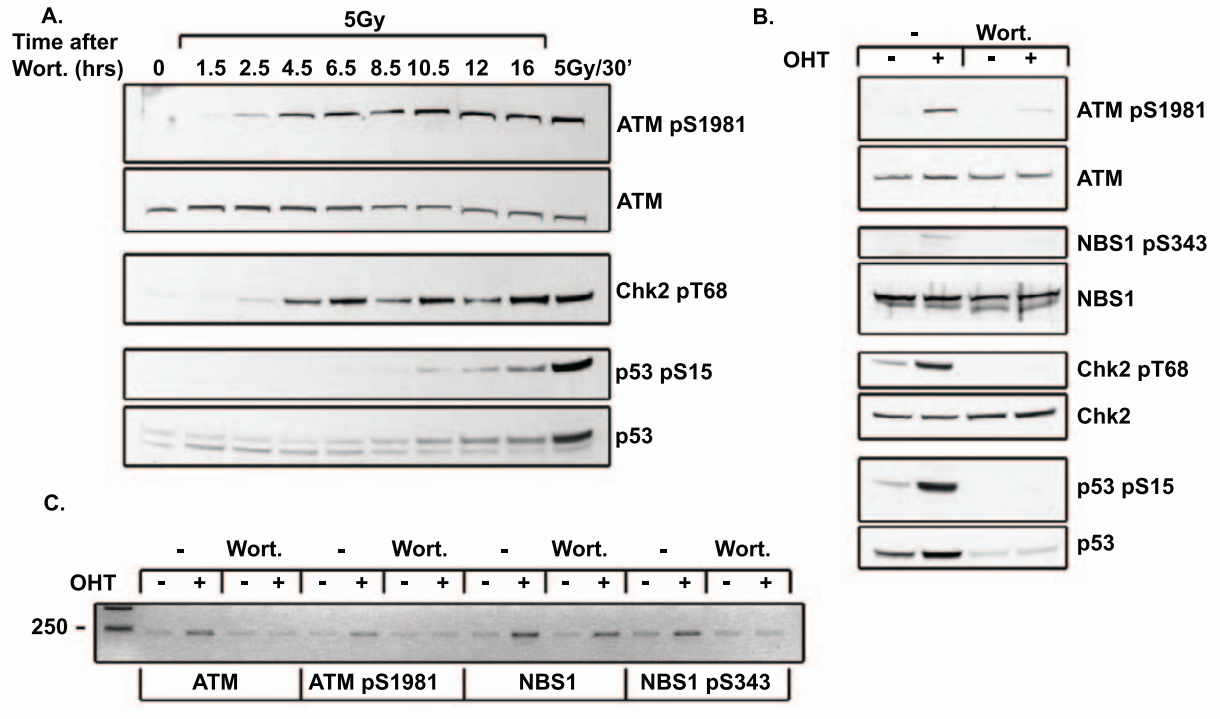

Figure S2: Wortmannin inhibits detection of ATM at a site-specific DSB. **A.** Wortmannin inhibition of ATM is short-lived in cultured cells. Wortmannin was added to MCF7 cells at time '0'. Cells were exposed to 5 Gy γ IR at the indicated times after wortmannin addition, then harvested 30 min after IR for Western blot analysis of the indicated proteins. 5Gy/30min – cells serving as positive control irradiated at 5Gy and collected 30 min after IR without addition of wortmannin. In order to continuously inhibit ATM activity over the course of these experiments, wortamannin was added to the cultures every two hours. **B.** MCF7 cells infected with HA-ER-I-PpoI were induced with 4-OHT in the presence or absence of wortmannin (30μM added every 2 hrs per Supplemental Fig. 3A). Cells were harvested at 8 hrs for Western blot analysis of the indicated proteins. **C.** MCF7 cells infected with HA-ER-I-PpoI were induced in the presence or absence of wortmannin (30μM added every 2 hrs) for a total of 8 hrs. Cells were then fixed and used for ChIP analysis at the rDNA site (489bp 3' to I-PpoI cut site).

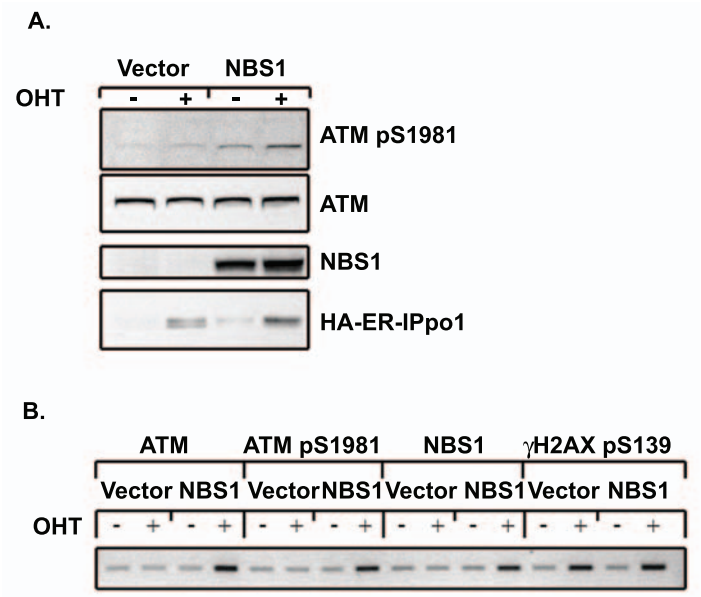

Figure S3: NBS1 is required for localization of activated ATM at DSBs. **A.** NBS1-deficient ILB1 cells complemented with p95(NBS1) or with a vector control were infected with HA-ER-I-PpoI retrovirus. Cells were induced with 4-OHT for 16hrs, then collected for Western blot analysis of the indicated proteins. **B.** Same as A. 16hrs after 4-OHT induction, cells were fixed and used in a ChIP assay.

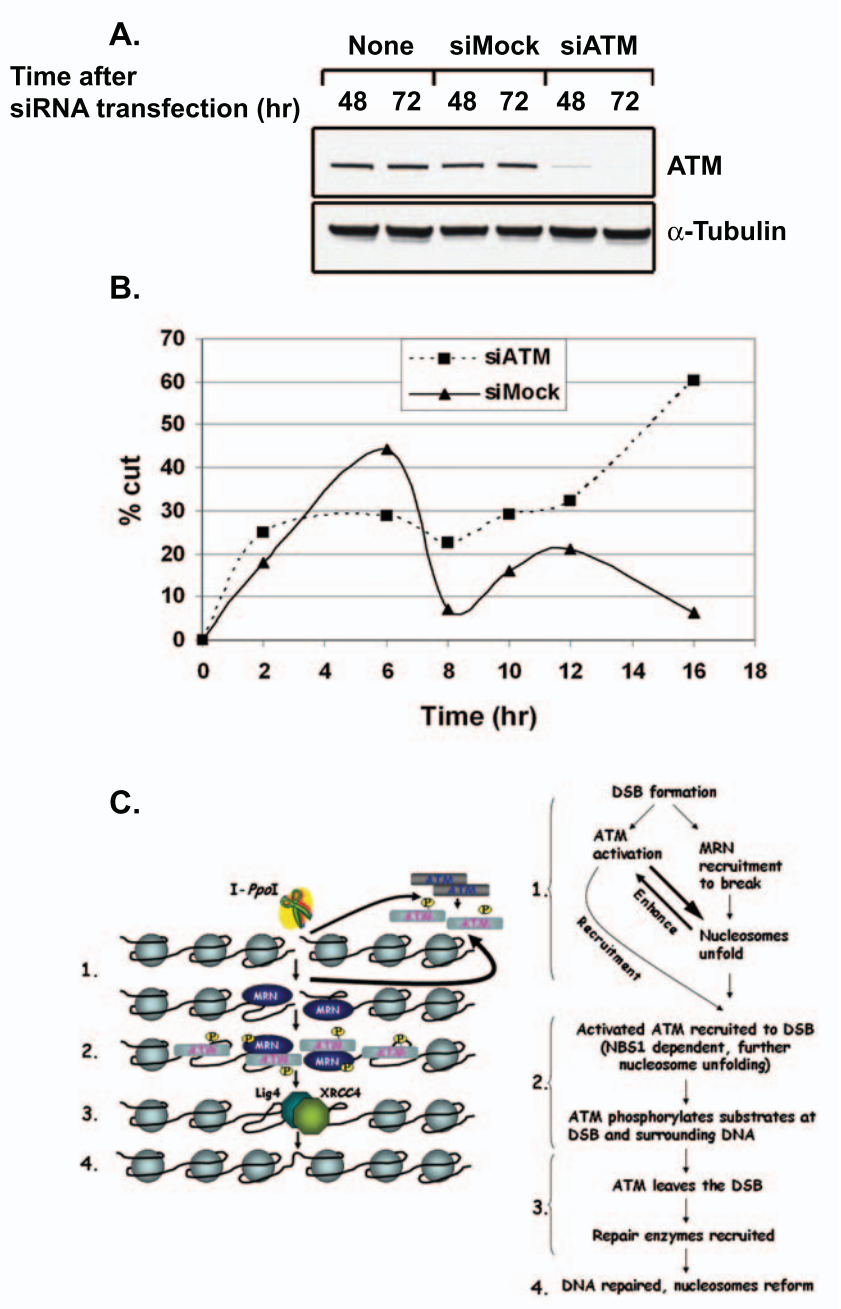

Figure S4: siRNA-mediated depletion of ATM results in a DSB repair defect. **A.** MCF7 cells were transfected with ATM-targeted siRNA. Cells were collected for Western blot analysis of the indicated proteins at 48 hrs or 72hrs after transfection.**B.** MCF7 cells were transfected with ATM-targeted siRNA, and 24hrs after transfection cells were infected with HA-ER-I-PpoI retrovirus. 24 hrs after infection cells were serum-starved for additional 24hrs, then induced with 4-OHT for the indicated times. Input DNA was prepared according to the ChIP protocol and used in real-time PCR to detect and quantify DSBs at the I-PpoI site on chromosome 1 as shown in Fig 3D. **C.** DSB detection and repair model. Site-specific DSB induction leads to a chromatin structural change that initiates ATM activation. Independently, the MRN complex binds to the DSB and further remodels chromatin with histone H2B loss to fully activate ATM (1), and then recruits activated ATM (2) to the DSB and surrounding DNA. Activated ATM recruited to the DSB site is then able to phosphorylate additional proteins at the DSB such as NBS1, and proteins adjacent to the break site such as H2AX (2). This recruitment of ATM further enhances nucleosome unfolding and histone loss at the DSB site (2). Repair proteins such as XRCC4 are recruited to the DSB as activated ATM leaves the DSB site (3,4). Though ATM leaves the DSB site, it remains bound to DNA surrounding the DSB site, perhaps to continue to phosphorylate substrates in these surrounding regions.

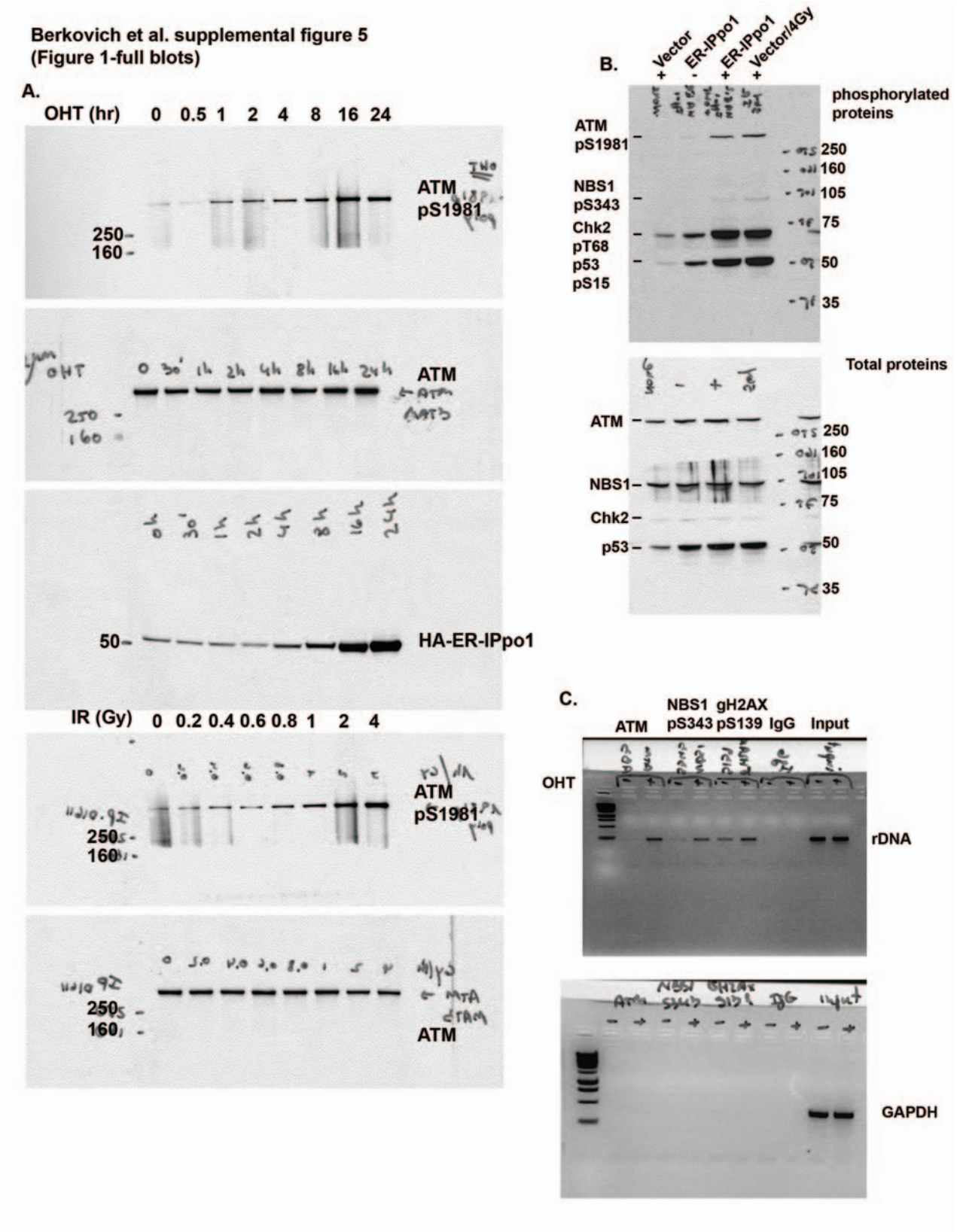

Berkovich et al. supplemental figure 5
Figure 1-full blots (cont.)

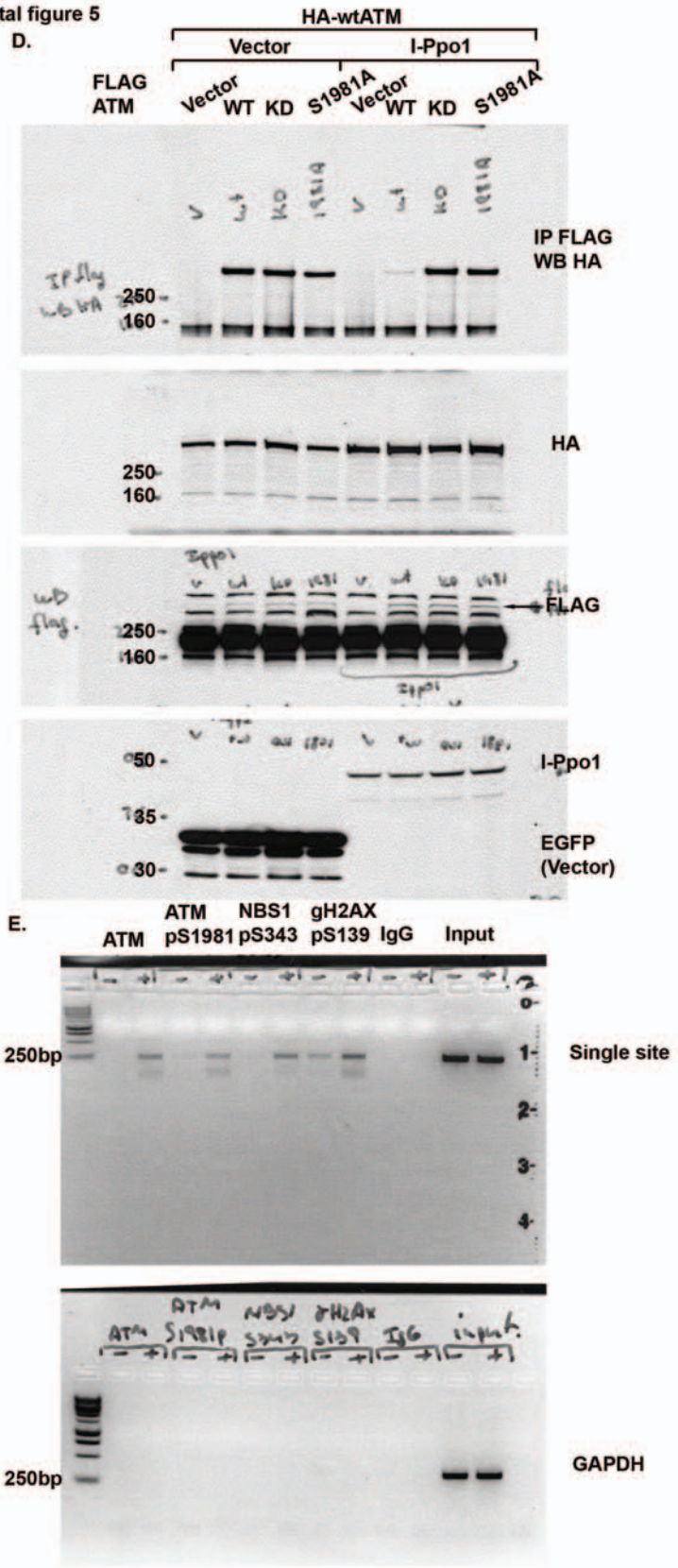

Berkovich et al. supplemental figure 5
Figure 2-full blots

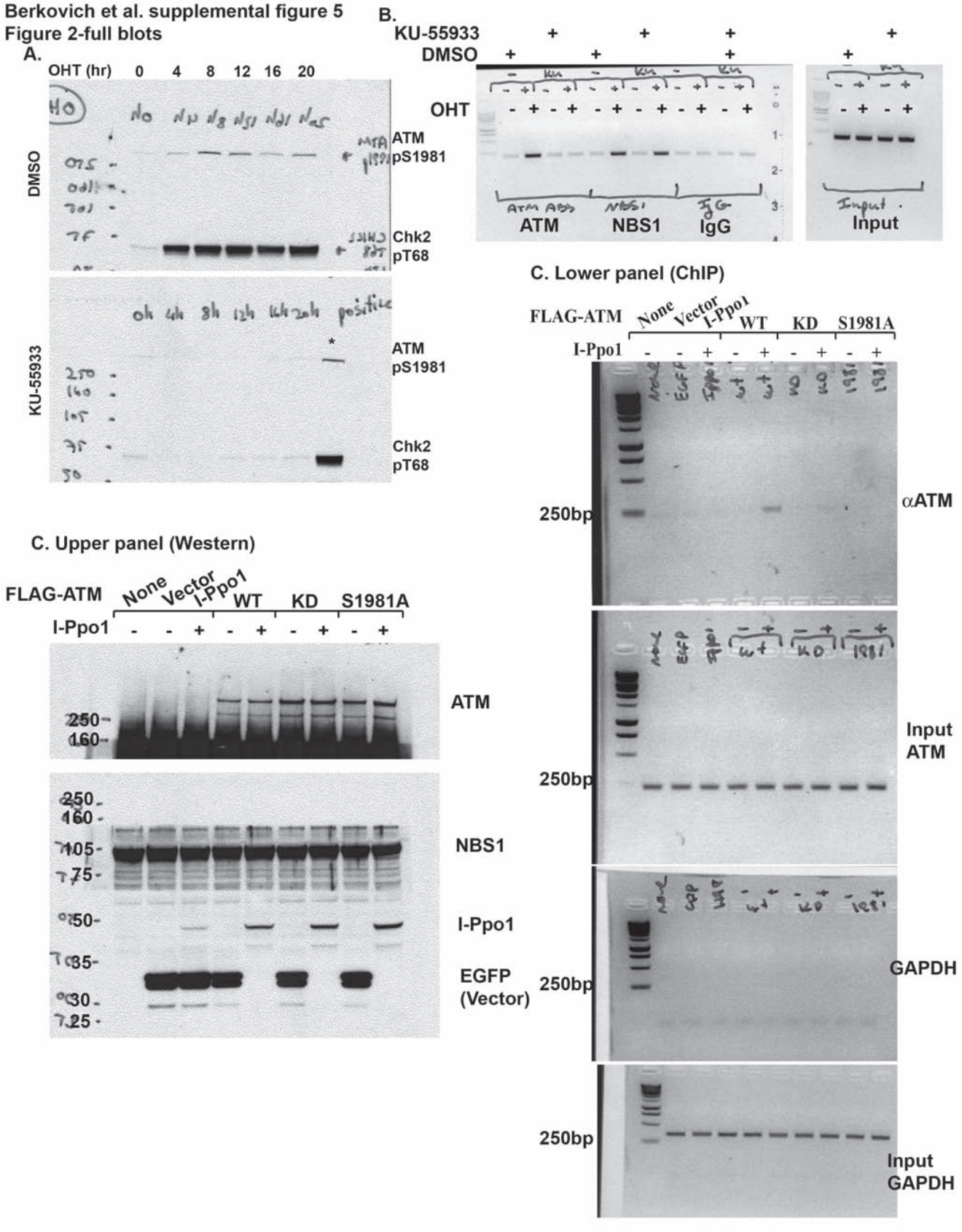

Berkovich et al. supplemental figure 5
Figure 3-full blots